

Analytical Approximation of Complex Band Structures for Band-to-Band Tunneling Models

Ximeng Guan*, Donghyun Kim, Krishna C. Saraswat, and H.-S. Philip Wong

Department of Electrical Engineering and Center for Integrated Systems

Stanford University

Stanford, CA 94305, USA

*E-mail: ximeng@stanford.edu

Abstract—A unified analytical expression is developed to accurately describe the complex band structures in commonly used diamond and zinc-blende semiconductors. Fitting the model to the numerical complex band structures shows a significantly improved accuracy as compared with the effective mass approximation. The model is used to study the band-to-band tunneling in Si, Ge, GaAs and GaSb, with a maximum error of <1.4% compared to the numerical band structures.

Keywords—complex band structure; band-to-band tunneling; non-parabolic approximation; effective mass approximation;

I. INTRODUCTION

Accurate modeling of band-to-band tunneling (BtBT) current is critical for the design of both high-performance nano-scale MOSFETs with low Ioff and energy-efficient tunneling transistors (TFET) with high Ion. Theoretically, an electron travels in an evanescent decaying mode when it tunnels through a forbidden gap, featuring a complex wave vector along the tunneling direction. The knowledge of these evanescent modes (i.e., complex band structure) therefore forms the basis of BtBT analysis, either in the construction of Green's-function-based numerical simulator [1] or in the derivation of action-integral-based analytical models [2]. Despite various numerical methods developed in the past decades [1,3-5], a unified analytical expression which provides quick and accurate access to the complex band structure of common semiconductors is highly attractive to both continuity-equation-based device simulator [6] and compact models. In this work, such analytical model is developed and calibrated, which captures both the direct and indirect tunneling modes along various directions of common semiconducting materials. With a maximum error of <1.4%, the model shows a significant improvement over the effective mass approximation.

II. MODELING APPROACH

A. Crystal Coordinates and Device Coordinates

The band-to-band tunneling direction is along the electric field, which may not necessarily be aligned with the principal axes (e.g., [100], [010] and [001]) defined in a bulk crystal. Since the imaginary wave number is defined only along the tunneling direction, transforming it into the crystal coordinate

system may result in more than one complex component. To facilitate the discussion and representation of the complex band structures, it is preferable to show the E - k dispersion relations in a coordinate system in which only one directional component of the wave vector is complex. Therefore besides the normal crystal coordinate system in which a wave vector is decomposed among the (x, y, z) directions, we introduce a device coordinate system in which a wave vector is decomposed among the tunneling direction, as denoted by \perp , and the directions perpendicular to the tunneling, as denoted by \parallel . Within this device coordinate system, the electron momentum perpendicular to the tunneling direction are conserved, with the components of wave vectors to be real. The 3D wave vector therefore takes the form of $(k_{\perp} + i\kappa_{\perp}, k_{\parallel}^1, k_{\parallel}^2)$, where $k_{\perp}, \kappa_{\perp}, k_{\parallel}^1$, and k_{\parallel}^2 are real numbers. Transformation between the two coordinate systems can be achieved by the rotation of axes, which is characterized by a 3-by-3 matrix relating (k_x, k_y, k_z) and $(k_{\perp} + i\kappa_{\perp}, k_{\parallel}^1, k_{\parallel}^2)$.

B. Analytical Approximations of Complex Band Structures

Detailed derivation of our analytical forms and its implications are described elsewhere in [7], in which a non-parabolic two-band $k \cdot p$ model is generalized to the case where electrons and holes have different effective masses. The results are summarized by (1) for the direct complex branch at Γ and (2) for the indirect complex branch stemming from an indirect valley α .

$$\kappa_{\Gamma\perp} = \begin{cases} 1/\hbar\sqrt{2m_v E [1 - E/(2E_{q\Gamma})]}, & 0 < E < E_{q\Gamma} \\ 1/\hbar\sqrt{2m_c (E_{g\Gamma} - E) [1 - (E_{g\Gamma} - E)/(2E_{g\Gamma} - 2E_{q\Gamma})]}, & E_{q\Gamma} \leq E < E_{g\Gamma} \end{cases}, \quad (1)$$

with $E_{q\Gamma} = E_{g\Gamma} m_c / (m_c + m_v)$

$$\kappa_{\alpha\perp} = \frac{1}{\hbar} \sqrt{2m_{c\alpha} (E_{c\alpha} - E) [1 - (E_{c\alpha} - E)/(2E_{\alpha} - 2E_{q\alpha})]}, \quad (2)$$

$E_{c\alpha} - E_{\alpha} + E_{q\alpha} < E < E_{c\alpha}, \alpha = \Delta(\text{Si}), L(\text{Ge})$

This work is supported in part by the Center for Energy Efficient Electronics Science (E3S), an NSF funded Science and Technology Center, and the member companies of the Initiative for Nanoscale Materials and Processes (INMP) at Stanford.

In (1) and (2), \mathcal{K} is the imaginary part of the component of the wave vector along the tunneling direction (\perp). m_c (m_v) is the electron (hole) effective mass at the conduction band minimum (valence band maximum) at Γ . $m_{c\alpha}$ is the electron effective mass at the indirect conduction band valley labeled α (α being L for Ge and Δ for Si.). All the effective masses are along the tunneling direction. The energy reference is set at the top of the valence band at Γ . $E_{g\Gamma}$ is the conduction band minimum at Γ , or the direct gap of the real band structure. $E_{c\alpha}$ is the indirect conduction band minimum at α , or the indirect gap of the real band structure. E_α is the energy difference between the conduction band minimum at α , where the indirect complex branch starts, and the state in the valence band where the same complex branch ends. Eq. (2) only describes the conduction branch of the complex band at α , because the valence branch for which $E < E_{c\alpha} - E_\alpha + E_{q\alpha}$ is usually far from the band gap region and therefore does not affect the indirect BtBT. Note that for the indirect complex branch described by (2), the wave vector may also have a real component along \perp , depending on the value of k_\perp at α (see for example, Fig. 4). This real component is irrelevant in the calculation of the action integral in (3) and therefore not described.

Both (1) and (2) are elliptic and *analytically integrable*, with effective masses m_c , m_v , $m_{c\alpha}$ and energy $E_{q\alpha}$ treated as fitting parameters. The direct bandgap at Γ ($E_{g\Gamma}$), the indirect band gap at the conduction valley α ($E_{c\alpha}$), and the energy range of the complex branch stemming from the valley (E_α) are fixed constants for a given material.

For direct tunneling at Γ , the wave number is purely imaginary and (1) is used to fit its imaginary part in the band gap. For indirect (i.e., phonon assisted) tunneling from Γ to the lowest conduction valley, the valence branch of the complex band stemming from Γ is given by Eq. (1), while the imaginary part of the conduction branch stemming from the valley is given by Eq. (2).

In the case when $E \rightarrow 0$ (or $E \rightarrow E_g$), the 2nd-order term of E (or $E_g - E$) can be neglected. Equation (1) therefore reverts to the conventional parabolic approximation. Similar asymptotic behavior is found in (2) when $E \rightarrow E_{c\alpha}$. $\mathcal{K}_{\Gamma\perp}$ approaches its maximum when $E \rightarrow E_{q\Gamma}$. The conduction branch and the valence branch of the complex band are connected smoothly at this point, revealing the inherent elliptic nature of the complex band.

C. Numerical Band Structures and Fitting Method

To fit the parameters in (1) and (2), the $sp^3d^5s^*$ tight-binding model [8-10] and a zone unfolding technique [11] are used to numerically generate complex band structures of semiconductors along selected orientations [5]. For each orientation, the most relevant complex branches are selected as fitting target according to the position and shape of the conduction band valleys. Fitting errors are estimated by the difference of calculated wave vectors at all energy levels of

interest. A genetic algorithm [12] is invoked to minimize the error and fit the parameters.

III. RESULTS AND DISCUSSIONS

A. Numerical Results of Complex Band Structures

The numerically calculated complex band structures along [100] of bulk Si and Ge are shown in Fig. 1. While the black curves are the real band structures corresponding to the propagating modes in the crystal, the red curves with imaginary wave vectors correspond to the decaying (tunneling) modes along the tunneling direction. Theoretical analysis shows that in both direct and indirect BtBT, the inverse of the inter-band tunneling probability (T) depends exponentially on the area of the region enclosed by the imaginary branch connecting the two real bands [13]-[15]. With the Wentzel-Kramers-Brillouin (WKB) approximation, this is described by [15]

$$T \propto \exp \left[-2 \int_{x_1}^{x_2} \kappa(E + Fx) dx \right] = \exp \left[-\frac{2}{F} \int_0^{E_{g\Gamma/c\alpha}} \kappa(E) dE \right] \quad (3)$$

where x_1 and x_2 are the classic turning points at which $\kappa = 0$. $E_{g\Gamma}$ ($E_{c\alpha}$) is the conduction band minimum at Γ (α). According to this dependence, it is observed that the major

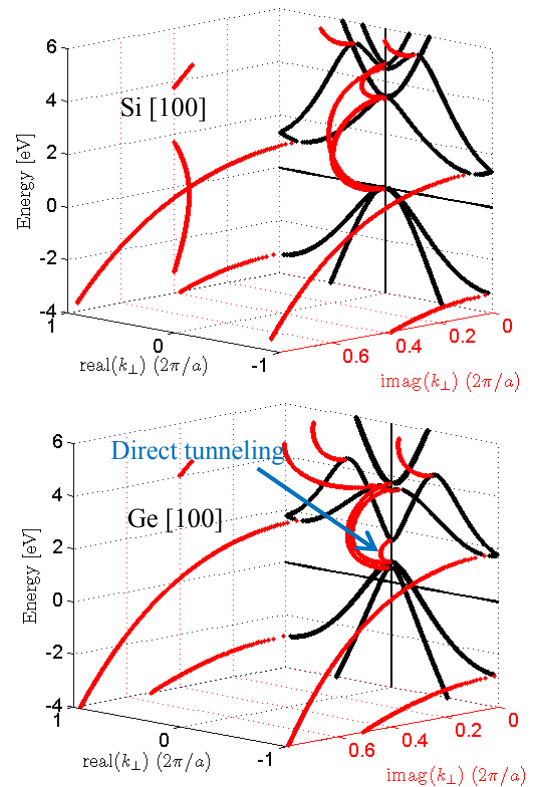


Figure 1. Complex band structures along [100] for bulk Si and Ge. While black curves are the normal band structure, the red curves correspond to the inter-band tunneling modes (i.e., complex band structures) along [100]. The indirect (phonon-assisted) tunneling dominates in the case of Si, while a direct tunneling path cannot be neglected for Ge.

BtBT mechanism in Si is the phonon-assisted indirect tunneling, while in Ge, due to the small direct gap at Γ , direct tunneling may take over the indirect tunneling and become the dominant mechanism under strong bias conditions. Similar observation has also been obtained from a numerical simulation using the non-equilibrium Green's function method [2]. With this observation and the exponential dependence by (3), it is concluded that the complex branches near the band gap region are the critical part of the entire band structures to BtBT which needs to be described with sufficient accuracy. Further investigation of these complex energy branches in different semiconductors reveals the fact that they are all close to the elliptic relation implied by a simple two-band model [7][13]. This opens up the possibility to use the analytical model in (1) and (2) as a reasonable approximation to the complex energy branches.

B. Parabolic and Non-Parabolic Approximations

Fig. 2 compares the parabolic model and our non-parabolic model for the direct and indirect tunneling trajectories in Ge. While our elliptic model agrees with the numerical results well, the parabolic approximation used by the effective mass approach overestimates the action integral by 20% for direct and 30% for indirect tunneling, which, when substituted into (3), translates to an underestimation of T by 70% and 80% when a constant field of 10^6 V/cm is present [7]. This is due to the fact that the parabolic approximation fails to capture the elliptic property of the complex band structure, which is prominent at the point where the conduction and valence branches join.

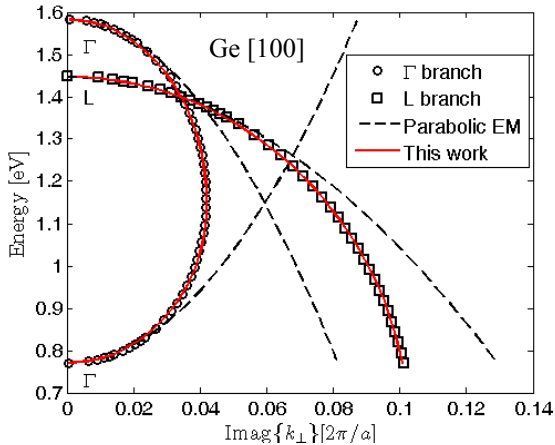


Figure 2. Comparison between the parabolic effective mass approach and our analytical approach for approximating the tunneling modes of Ge along the [100] orientation. In both cases of direct and indirect tunneling, the parabolic approximation tends to overestimate the action integral and therefore underestimate the tunneling probability [7].

C. Material Characterization

Fig. 3 compares the direct tunneling trajectories among Ge, GaAs and GaSb. It is observed that for both large-gap and small-gap materials, and along typical orientations in the semiconductors, the complex branches that join the conduction band minimum and the valence band maximum are all close in shape to ellipsoids, showing the universality of our analytical model as applied to different semiconductors.

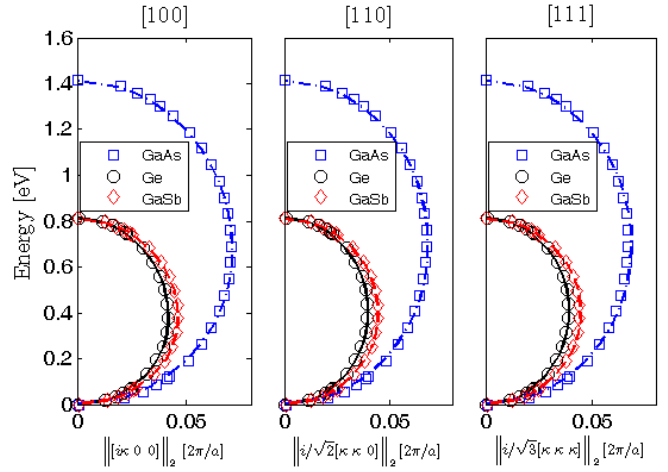


Figure 3. Direct tunneling modes along [100], [110] and [111] in bulk GaAs, Ge and GaSb. The symbols are the numerical results and the curves are from our analytical approximation.

Fig. 4 compares the direct/indirect tunneling trajectories in Ge and Si. While the action integral for direct (Γ) and indirect tunneling (Γ -L) can be close for Ge devices, showing a possible transition from indirect to direct tunneling under strong electric field, the indirect (Γ - Δ) tunneling is the most probable BtBT mechanism in Si due to its large direct gap. The elliptic model captures both the close loop of the direct tunneling trajectory at

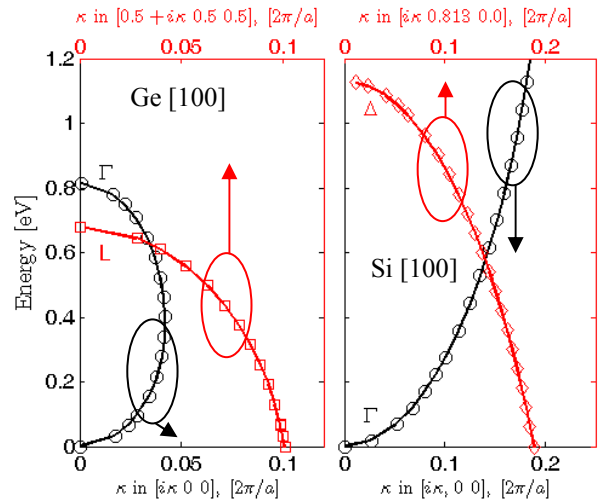


Figure 4. Indirect tunneling modes along the [100] orientation in Ge (left) and Si (right). The symbols are the numerical results and the curves are from our analytical approximation.

Γ and the open trajectory for indirect tunneling at L and Δ within the energy region of interest.

Fig. 5 compares the complex band structures of Ge and Si, stemming from their respective real conduction band minima. Note that along each direction, only the valleys that give the lowest effective mass are selected. The [110] direction has the smallest effective mass in both materials, because at least one of the valleys (L [1 -1 1] in Ge and X [001] in Si) shows transverse effective mass along [110]. The largest effective masses turn out to be along [100] in Ge and [111] in Si, since no valleys show transverse effective mass along these directions.

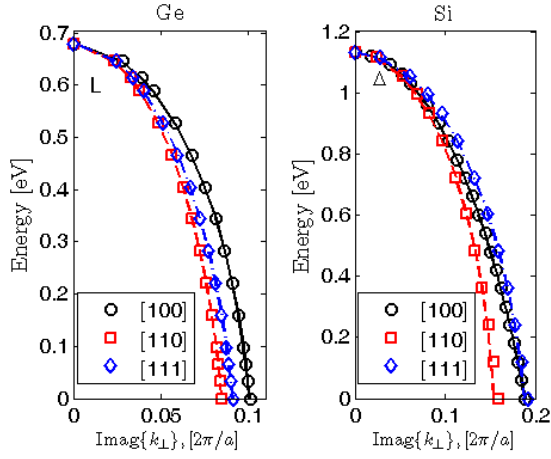


Figure 5. Lowest conduction branches of tunneling modes along different orientations in Ge at L (left) and Si along Δ (right). Symbols are numerical results and curves are analytical fittings to the symbols. While both materials have the smallest value of action integral along [110], the largest value of action integral is along different orientations in the two semiconductors.

D. Parametrization of the Model

Tables 1 and 2 list the fitted parameters of (1) and (2) for Ge, GaAs, GaSb and Si along different directions. The fitting errors are within 1.4% along all directions of these materials, which translates into a maximum error of T of less than 6% when a constant field of 10^6 V/cm is present.

TABLE I. FITTED m_c AND m_v VALUES FOR (1) AT Γ FOR THE DIRECT TUNNELING MODES OF Ge, GaAs and GaSb. VALENCE BRANCH OF Si IS ALSO FITTED FOR INDIRECT TUNNELING [7].

	$m_c (m_0)$	$m_v (m_0)$	$E_{g\Gamma} (eV)$	Fit. Err.
Ge [100]	0.038	0.044	0.814	0.78%
Ge [110]	0.037	0.037	0.814	1.09%
Ge [111]	0.036	0.035	0.814	1.21%
GaAs [100]	0.064	0.072	1.416	0.96%
GaAs [110]	0.061	0.064	1.416	1.32%
GaAs [111]	0.061	0.062	1.416	1.40%
GaSb [100]	0.041	0.046	0.811	0.56%
GaSb [110]	0.039	0.041	0.811	0.76%
GaSb [111]	0.039	0.040	0.811	0.81%
Si [100]	0.370	0.201	3.398	0.29%
Si [110]	0.113	0.123	3.398	0.62%
Si [111]	0.121	0.109	3.398	0.66%

IV. CONCLUSIONS

An analytically integrable model of complex band structures is developed to capture the inter-band tunneling modes in common semiconductors. The elliptic nature of the model allows accurate fitting to the numerical results within an

error of 1.4%. The model improves the understanding of complex band structures and enables further development of both accurate BtBT models for device simulation and compact modeling of tunneling current.

TABLE II. FITTED E_{ca} AND E_{qa} VALUES FOR (2). (THE INDIRECT TUNNELING MODES OF Ge AND Si AT THEIR RESPECTIVE CONDUCTION BAND MINIMA.) ENERGY REFERENCE FOR E_{ca} IS SET AT THE VALENCE BAND MAXIMA. E_a IS THE ESTIMATED ENERGY RANGE OF THE COMPLEX BRANCH AT THE L (Ge) OR Δ (Si) VALLEY. [7]

	$m_{ca} (m_0)$	E_{ca}	$E_{qa}(eV)$	$E_a(eV)$	Fit. Err.
Ge@L [100]	0.116	0.678	1.081	1.940	0.24%
Ge@L [110]	0.080	0.678	1.035	1.940	0.16%
Ge@L [111]	0.090	0.678	0.993	1.940	0.12%
Si@Δ [100]	0.202	1.131	1.451	4.223	0.07%
Si@Δ [110]	0.185	1.131	2.865	4.223	1.27%
Si@Δ [111]	0.256	1.131	2.701	4.223	0.83%

REFERENCES

- [1] M. Luisier, A. Schenk, and W. Fichtner, "Atomistic simulation of nanowire in the sp3d5s* tight-binding formalism: From boundary conditions to strain calculations," Phys. Rev. B., vol. 74, 205323, 2006.
- [2] M. Luisier, and G. Klimeck, "Simulation of nanowire tunneling transistors: from the Wentzel-Kramers-Brillouin approximation to full-band phonon-assisted tunneling," J. Appl. Phys., vol. 107, 084507, 2010.
- [3] Y. C. Chang, and J. N. Schulman, "Complex band structures of crystalline solids: an eigenvalue method," Phys. Rev. B., vol. 25, pp. 3975-3986, 1982.
- [4] J. K. Tomfohr and O. F. Sankey, "Complex band structure, decay lengths, and Fermi level alignment in simple molecular electronic systems," Phys. Rev. B, vol. 65, 245105, 2002.
- [5] S. E. Laux, "Computation of complex band structures in bulk and confined structures," Proc. 13th Int. Workshop Comput. Electron., pp. 1-4, 2009.
- [6] M. R. Pinto, C. S. Rafferty, and R. W. Dutton, PISCES-II User's Manual, Stanford, 1984.
- [7] X. Guan, D. Kim, K. C. Saraswat, and H.-S. P. Wong, "Complex band structures: from parabolic to elliptic approximation," IEEE Electron Device Lett., in press.
- [8] J.-M. Jancu, R. Scholz, F. Beltram, and F. Bassani, "Empirical sp3d5s* tight-binding calculation for cubic semiconductors: General method and material parameters," Phys. Rev. B., vol. 57, pp. 6493-6507, 1998.
- [9] T. B. Boykin, G. Klimeck, and F. Oyafuso, "Valence band effective-mass expressions in the sp3d5s* empirical tight-binding model applied to a Si and Ge parametrization," Phys. Rev. B, vol. 69, 115201, 2004.
- [10] T. B. Boykin, G. Klimeck, R. C. Bowen, and F. Oyafuso, "Diagonal parameter shifts due to the nearest-neighbor displacements in empirical tight-binding theory," Phys. Rev. B., vol. 66, 125207, 2002.
- [11] T. B. Boykin, and G. Klimeck, "Practical application of zone-folding concepts in tight-binding calculations," Phys. Rev. B., vol. 71, 115215, 2005.
- [12] Global Optimization Toolbox 3 User's Guide, The Mathworks Inc., 2011.
- [13] E. O. Kane, "Zener tunneling in semiconductors," J. Phys. Chem. Solids, vol. 12, pp. 181-188, 1959.
- [14] D. Kim, "Theoretical performance evaluations of NMOS double gate FETs with high mobility materials: strained III-V, Ge and Si," PhD dissertation, Stanford, 2009.
- [15] S. M. Sze and Kwok, K. Ng, Physics of Semiconductor Devices, John Wiley and Sons, Inc., p. 424-428, 2007.